

Energy & Environmental Science

Accepted Manuscript



This is an *Accepted Manuscript*, which has been through the Royal Society of Chemistry peer review process and has been accepted for publication.

Accepted Manuscripts are published online shortly after acceptance, before technical editing, formatting and proof reading. Using this free service, authors can make their results available to the community, in citable form, before we publish the edited article. We will replace this *Accepted Manuscript* with the edited and formatted *Advance Article* as soon as it is available.

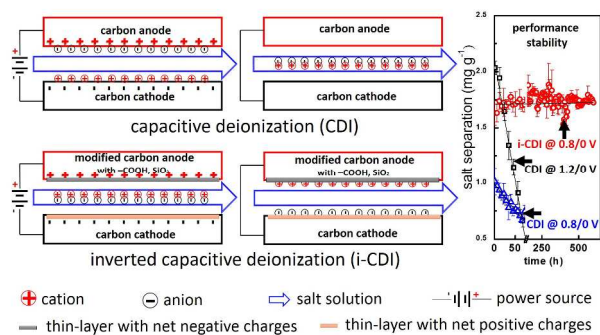
You can find more information about *Accepted Manuscripts* in the [Information for Authors](#).

Please note that technical editing may introduce minor changes to the text and/or graphics, which may alter content. The journal's standard [Terms & Conditions](#) and the [Ethical guidelines](#) still apply. In no event shall the Royal Society of Chemistry be held responsible for any errors or omissions in this *Accepted Manuscript* or any consequences arising from the use of any information it contains.

Broader Context

Capacitive deionization (CDI) is an emerging technology that can reduce the energy cost of salt removal for a variety of water streams. Previous studies have shown the loss of salt separation during operation of a CDI cell, which was due to oxidation of the anode in an aqueous solution. While oxidation-resistant anode materials have been suggested, they have yet to be developed for the improvement of CDI performance stability. To overcome this difficulty, carbon electrodes with completely different surface charge states were employed to develop a novel desalination system, called the inverted capacitive deionization (i-CDI) system. Operation of this system results in salt desorption when the cell is charged using a power supply and salt adsorption when the cell is shorted. Through this study, salt separation performance of the i-CDI system can be further improved by enhancing the net surface charges of carbon materials. This enhancement can be achieved through the relationship between the zeta potential of oxides and the potential of the zero charge for carbon electrodes (Eq. [3] in the main text) with broad applicability in other fields, *e.g.*, capacitive mixing for energy extraction.

Table of Contents (ToC)



To enhance performance stability, carbon electrodes with opposite net surface charges were employed to develop the inverted capacitive deionization system.

Surface Charge Enhanced Carbon Electrodes for Stable and Efficient Capacitive Deionization Using Inverted Adsorption-Desorption Behavior

Xin Gao,^a Ayokunle Omosebi,^a James Landon,^{a*} and Kunlei Liu,^{ab*}

^aCenter for Applied Energy Research, University of Kentucky, Lexington, KY 40511, USA.

^bDepartment of Mechanical Engineering, University of Kentucky, Lexington, KY 40506, USA.

Email: James.Landon@uky.edu; Fax: +1 859 257 0302; Tel: +1 859 257 0349.

Email: Kunlei.Liu@uky.edu; Fax: +1 859 257 0302; Tel: +1 859 257 0293.

Abstract

Unsustainable and inefficient capacitive deionization (CDI) performance has been observed through CDI operation with carbon xerogel (CX) electrodes for 50 hours using a constant-voltage charging method. This behavior is primarily accounted for by changes in the surface chemistry for the studied material via oxidation of the carbon electrodes in an aqueous solution. In order to improve performance stability, we have developed a novel CDI system using an anode with net negative surface charges and a cathode with net positive surface charges. As a result, salt separation in this system is achieved in an opposing manner to the conventional CDI system, *e.g.*, when the system is charged using a power source, cations and anions are desorbed at the anode and cathode, respectively. This system is named the inverted capacitive deionization (i-CDI) system. Most importantly, salt separation in the i-CDI system was maintained for over 600 hours, which is approximately an increase of 530% in lifetime compared to a CDI system operated under similar conditions. This enhanced performance stability is attributed to the use of oxidized anodes in the i-CDI system, which limits the possibility for loss in separation performance due to carbon oxidation in an aqueous solution.

Key Words

capacitive deionization, performance stability, carbon oxidation, potential of zero charge (E_{PZC}), working voltage window

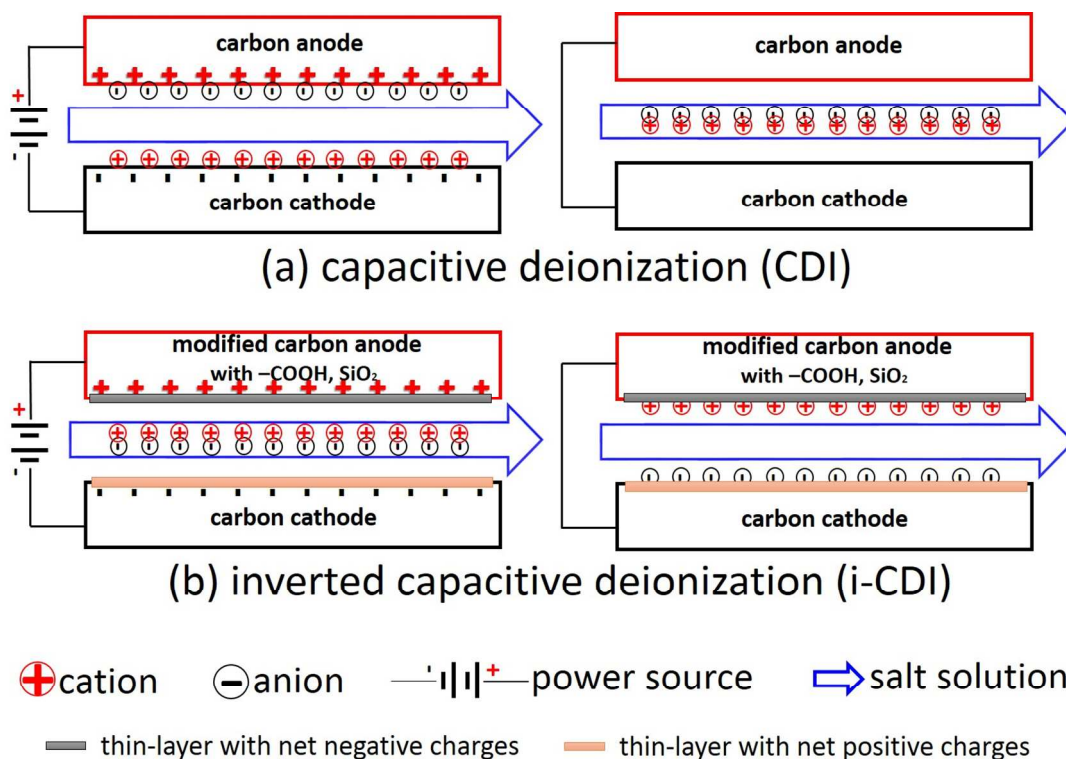


Figure 1. Schematic of (a) capacitive deionization (CDI) and (b) inverted capacitive deionization (i-CDI) systems. Both systems have the same physical structure where carbon cathodes and anodes are separated by a flowing salt solution. (It should be noted that the cathode and anode are defined as shown in the diagrams.) However, because the net surface charges on the carbon surface can be managed by chemical and/or electrochemical modifications, the i-CDI system shows completely opposite adsorption-desorption behavior compared to the conventional CDI system. For instance, when the i-CDI system is charged using a power source, cations and anions are desorbed at the anode and cathode, respectively, and when the i-CDI system is discharged under a short-circuit condition, cations and anions are adsorbed at the anode and cathode, respectively.

1. Introduction

Water, more specifically fresh water, is an essential component for human life.¹ While the earth is mostly covered by water, only limited fresh water is available and suitable for human consumption.² To meet fresh water requirements, desalination technologies have been developed to match population and industry growth, of which distillation, reverse osmosis, and electrodialysis are currently among the options used commercially to produce clean water.³ Capacitive deionization (CDI) is an alternative and maturing technology for desalination, which is based upon reversible salt adsorption-desorption at porous carbon electrodes.⁴⁻⁶ Research and development have been extensively performed in the preparation and modification of carbon materials,⁷⁻²⁰ the fabrication of new flow systems for CDI applications,²¹⁻²⁵ and the mathematical modeling of desalination in a CDI cell.^{5, 26-29} We expect that CDI technology may lead to a significant reduction in the operational and energy costs for desalination processes as no heat-treatment, high pressure, or membrane is required.^{4-6, 30}

Desalination in a CDI system is achieved by using an external power source to adsorb salts into the electric double layer (EDL) at the surface of a porous carbon electrode. As shown in Fig. 1(a), a typical CDI system has a structure such that a carbon cathode and anode are separated by a flowing salt solution. By applying a voltage (or a current) from an external power source to the cell, anions and cations in a salt solution are electrostatically attracted into the EDL at the polarized anode and cathode, respectively, resulting in salt being removed from the solution. Subsequently, by shorting the cathode and anode, due to the reduction in electrostatic attraction, the trapped ions are

released back into solution to form a concentrated stream, and the cathode and anode are correspondingly regenerated.

By using the above-mentioned CDI working principle, a few research groups have examined adsorption-desorption behavior of CDI cells for 50-500 hours using a constant-voltage charging method.³¹⁻³⁴ In these cases, cells were charged within a range of 0.7-1.2 V for adsorption and discharged at short-circuit for desorption. All of these studies depicted performance degradation with CDI cells assembled with commercially available activated carbon (AC) cloth and monolithic carbon xerogel (CX) electrodes in deaerated NaCl solutions. This performance loss is mainly attributed to oxidation at the anode via electrochemical reaction of the carbon electrodes in the aqueous solution, leading to the formation of oxide layers at the carbon surface.^{11, 32, 33, 35-37} As a consequence, these oxides (*e.g.*, carboxylic groups) bias the electrode into having a negatively charged surface state and/or a cation exchange behavior,^{4, 5, 11, 38} leading to not only changes in the point of zero charge (pH_{PZC}) at the carbon surface but also a relocation in the potential of zero charge (E_{PZC}) of the carbon electrode.³⁸⁻⁴⁸ Overall, these changes in surface charges mainly caused the loss in salt separation observed in these CDI cells.

In order to sustain desalination performance, oxidation at the anode needs to be managed in a CDI cell, correspondingly minimizing the E_{PZC} shift. Therefore, oxidation-resistant carbon materials need to be developed for CDI anodes,³³ and similar development has been conducted for carbon materials in the fuel cell field, where carbon oxidation is likewise a substantial problem.⁴⁹⁻⁵¹ However, prior studies have yet to resolve the issue of anode oxidation for CDI applications. To aid in the separation process, an alternative route would be to exploit the surface charges created in the CDI

cell *via* electrochemical oxidation. For instance, the oxidized CDI anode will have net negative surface charges due to the formation of $-\text{COO}^-$ groups from the hydrolysis of $-\text{COOH}$ groups. These negative surface charges can facilitate cation adsorption during the CDI separation process.

By leveraging the impact of the E_{PZC} location (or net surface charges) on the electrosorption of salts in a CDI cell, and the phenomenon of chemical charging in a capacitive mixing (CAPMIX) cell,^{9, 44, 48, 52-57} we have developed an inverted capacitive deionization (i-CDI) system. Desalination in an i-CDI system is mainly achieved by a spontaneously formed EDL at a chemically-modified surface of a carbon electrode without an external power source. As shown in Fig. 1(b), the i-CDI system possesses fixed charges at an electrode's surface to spontaneously adsorb ions while an applied voltage from an external power source is used to desorb ions. To demonstrate this concept, the i-CDI system in this study employed carbon electrodes with functionalized/oxidized carbon as the anode and pristine carbon as the cathode. (It should be noted that we have defined the anode as the electrode where positive potential is applied and the cathode as the electrode where a negative potential is applied.)

The i-CDI system can lead to a significant improvement in the performance stability for long-term CDI operation owing to the mitigation of the problem for oxidation at the anode, as the anode in the i-CDI system in this example is already composed of an oxide layer to enhance cation adsorption. Therefore, we consider that use of this method is an alternative route to the development of oxidation resistant materials. In this paper, we will demonstrate the use of the i-CDI system to provide stable

separation performance for over 600 hours of operation and suggest methods for electrode development for i-CDI systems.

2. Experimental

2.1. Materials Preparations

Preparation of carbon materials has been documented in the literature.^{58, 59} In this study, we first prepared a solution by adding 20.00 ± 0.02 g resorcinol ($C_6H_6O_2$, Sigma-Aldrich), 29.48 ± 0.02 g formaldehyde (CH_2O , 37 wt% in methanol, Sigma-Aldrich), 6.32 ± 0.02 g of 0.02 M Na_2CO_3 solution (Sigma-Aldrich), and 6.00 ± 0.02 g of deionized H_2O in a sealed glass bottle. The solution was stirred for 30 min. The resulting solution was used to infiltrate a dry carbon cloth (untreated, Fuel Cell Earth). Subsequently, the wetted carbon cloth was immobilized between two glass slides, sealed with aluminum foil overnight, and heated at $85^\circ C$ for a period of 24 hours in air. A solvent-exchange process was performed for the polymerized sheets in which the sheets were subjected to soaking in deionized water, soaking in acetone, and air-drying. Time taken for each step was 2 hours. Finally, the dried sheets were carbonized using a quartz tube in a computer-controlled furnace (Lindberg M, Thermo Scientific), where the temperature was held at $1000^\circ C$ for 2 hours using a ramp rate of $5^\circ C \text{ min}^{-1}$ for both heating and cooling from room temperature under N_2 atmosphere. The resulting sheet is called pristine carbon xerogel (CX) with a density of $0.48 \pm 0.02 \text{ g cm}^{-3}$, a conductivity of $55 \pm 1 \text{ S cm}^{-1}$, and a thickness of $0.046 \pm 0.003 \text{ cm}$. For a comparison in desalination performance, commercially available monolithic carbon cloths with much higher microporosity,

Zorflex (ZX) and Spectracarb (SC), were purchased from Chemviron Carbon and Caplinq, respectively.

In order to prepare electrodes with a net negative surface charge and yet retain high porosity⁶⁰, tetraethyl orthosilicate (TEOS) (>99%, Sigma-Aldrich), ethanol (200 proof, Pharmco-Aaper), and HNO₃ (~70%, Acros) were vigorously mixed with a volumetric ratio of 1:20:1 for 1 hour. The pristine CX sheets were dipped once into the resulting solution for 30 min and heated at approximate 280°C in air (Fisher Scientific, Model 281) for another 72 hours. The resulting material is denoted by Si-CX in the text.

In order to identify shifts in the E_{PZC} of carbon materials, the pristine CX sheets were also modified using HNO₃ at various temperatures. Briefly, a graduated cylinder with a glass cover was used to heat 300 cm³ of HNO₃ (~70%, Acros) in a temperature-controlled coolant bath (Thermo Scientific). When the temperature of HNO₃ was stable at 20, 35, 50 and 80°C, a pristine CX sheet with a geometric area of ~50 cm² was placed into the cylinder for 1 hour. After treatment, to remove any residual HNO₃ on the surface of the carbon, the treated carbon was washed with a significant amount of deionized water until the pH value of wash solution approached neutral.

2.2. Materials Characterizations

Material characterizations were performed using a surface area and porosity analyzer (ASAP2020, Micromeritics) and a Fourier-transform infrared (FTIR) spectrometer (6700, Nicolet). Surface area and porosity were measured using ~150 mg of CX electrode after degassing at 160°C for at least 4 hours, and isotherms were recorded by N₂ adsorption-desorption at 77 K. FTIR spectra were recorded by co-adding 256 ‘scans’ at 4 cm⁻¹ resolution, and KBr was used as a background. Each FTIR sample was prepared with a

~70 mg mixture of CX/KBr at a ratio of 0.3 wt% (CX vs. KBr) where the prepared material was ground into a powder before mixing. In order to quantify the acidity of the oxidized CX materials, each sample of ~100 mg was immersed in 50 cm³ of 0.015 M NaOH solution for 72 hours, and the resulting NaOH was back titrated using 0.01 M H₂SO₄ in an automatic titration instrument (800 Dosino, Metrohm).

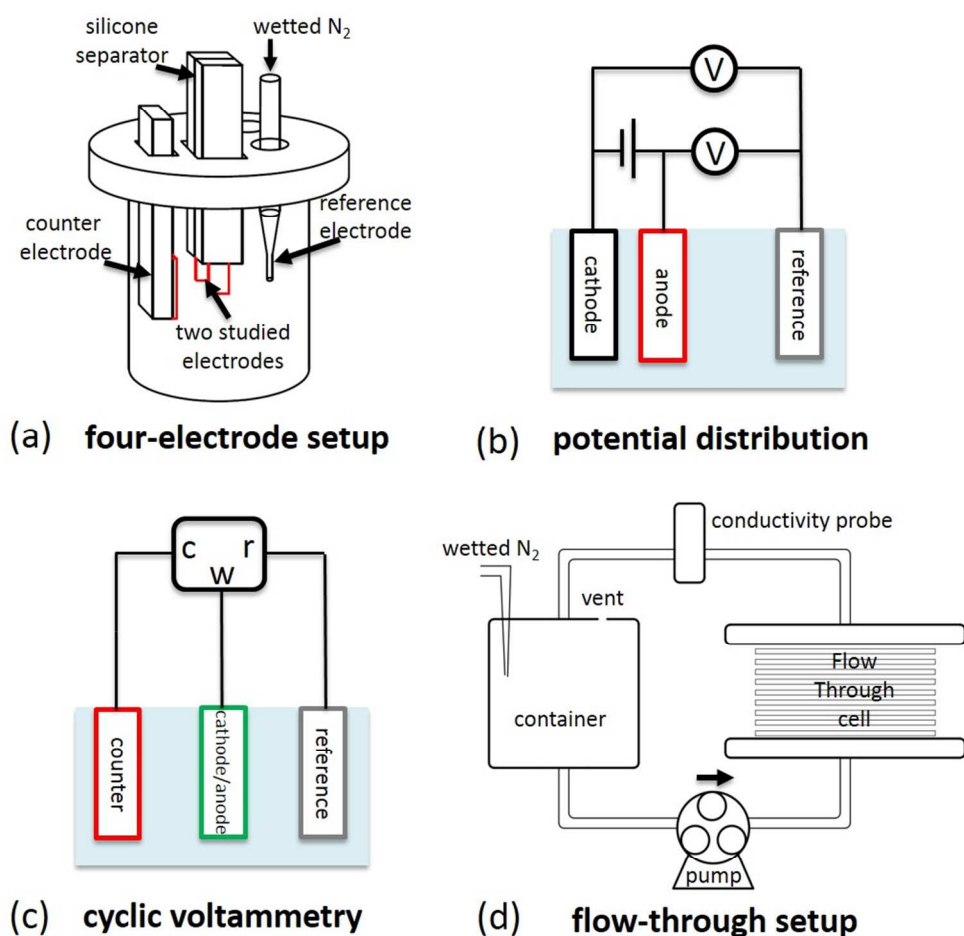


Figure 2. Schematic of the main experimental setup used for the i-CDI and CDI studies. (a) Potential distributions and cyclic voltammograms were studied using a four-electrode setup. (b) Use of the four-electrode cell to measure the potential distribution for a pair of electrodes. (c) Use of the four-electrode cell to detect the E_{PZC} via cyclic voltammetry. In this diagram, c, w, and r represent counter, working, and reference electrodes,

respectively. (d) Cycling performance of a CDI cell was examined using a flow-through cell system.

2.3. Electrochemical Characterizations Using a Four-Electrode Setup

In order to obtain comparable potential distribution data for the CDI cell under investigation in this study, a four-electrode setup was constructed. The four-electrode setup depicted in Fig. 2(a) consists of two studied carbon electrodes, a reference electrode, and a counter electrode. Each electrode was tightly placed in the cell such that the distance between the pair of studied electrodes was 0.15 cm (the same configuration used in the flow-through cell), and the distance between the tip of the saturated calomel reference electrode (SCE) and the studied electrode was around 1 cm. Each studied carbon electrode has an approximate geometric area of 0.36 cm². All tests except stated otherwise were performed in 4.3 mM deaerated NaCl solution.

The four-electrode setup possesses two functions. The first function shown in Fig. 2(b) was used to measure the potential distribution for the cathode and anode. Another function shown in Fig. 2(c) was used to detect the location of the E_{PZC} for each individual electrode using cyclic voltammetry. In detail, in Fig. 2(b), by shorting the two electrodes, the short-circuit potential *vs.* the SCE electrode was measured using a data logger (GL220, Graphtec). By applying a voltage using a power supply (E3632A, Agilent) across the cathode and anode, the potential drop across each electrode *vs.* the SCE electrode was measured again with the use of the same data logger. Subsequently, as shown in Fig. 2(c), each electrode was voltammetrically characterized via a conventional three-electrode connection using a potentiostat (Reference 600, Gamry Instruments) and

a counter CX electrode with geometric area of about 3.6 cm² for the E_{PZC} determination. The E_{PZC} and potential distribution measured in this work can be used as a tool to determine the locations of all system potentials. It is considered that these potentials will not change considerably if conditions remain constant (*e.g.*, stability of salt separation).

2.4. Adsorption-Desorption Cycling Test

Cycling tests were executed in the flow system shown in Fig. 2(d) where a flow-through cell, a conductivity sensor (19500-45, Cole-Parmer), a peristaltic pump (Masterflex L/S, Cole-Parmer), and a polyethylene tank were serially connected *via* silicone and polyethylene tubing (Fig. S1). Experimental automation and timing were facilitated with a computer-controlled relay box (Denkovi Assembly Electronics Ltd.). During operation, 31 L of 4.3 mM deaerated NaCl solution was circulated at 75 mL min⁻¹ through a cell assembled with 16 pairs of electrodes separated by 0.15 cm thick silicon rubber spacers. It should be noted that total mass of the CX electrodes including the carbon cloth substrates was about 16 g. Due to the large volume of salt solution used, the steady-state conductivity (σ) after the adsorption and desorption profiles is equivalent to the σ value for the bulk solution. Therefore, the electrosorption capacity (Γ) was quantified by the solution flow rate (Φ) multiplied by the integration of the conductivity curve with time (t) taken for both the adsorption and desorption steps (Eq. [1]).

$$\Gamma = K \Phi \int \sigma(t), \quad K = M / (k m) \quad [1]$$

where M is the molecular weight of the salt, m is the mass of the electrodes, and k (112.77 $\mu\text{S cm}^{-1} \text{ mM}^{-1}$) is the slope calculated from a calibration plot of conductivity *vs.* NaCl concentration. Similarly, the charge density (Q) during both the adsorption and

desorption steps was calculated by integration of the current curves. Finally, the charge efficiency (Λ) is the ratio of Γ (converted to equivalent charge using Faraday's constant (F)) to the charge density (Eq. [2]).

$$\Lambda = (\Gamma F / M)/(Q) \quad [2]$$

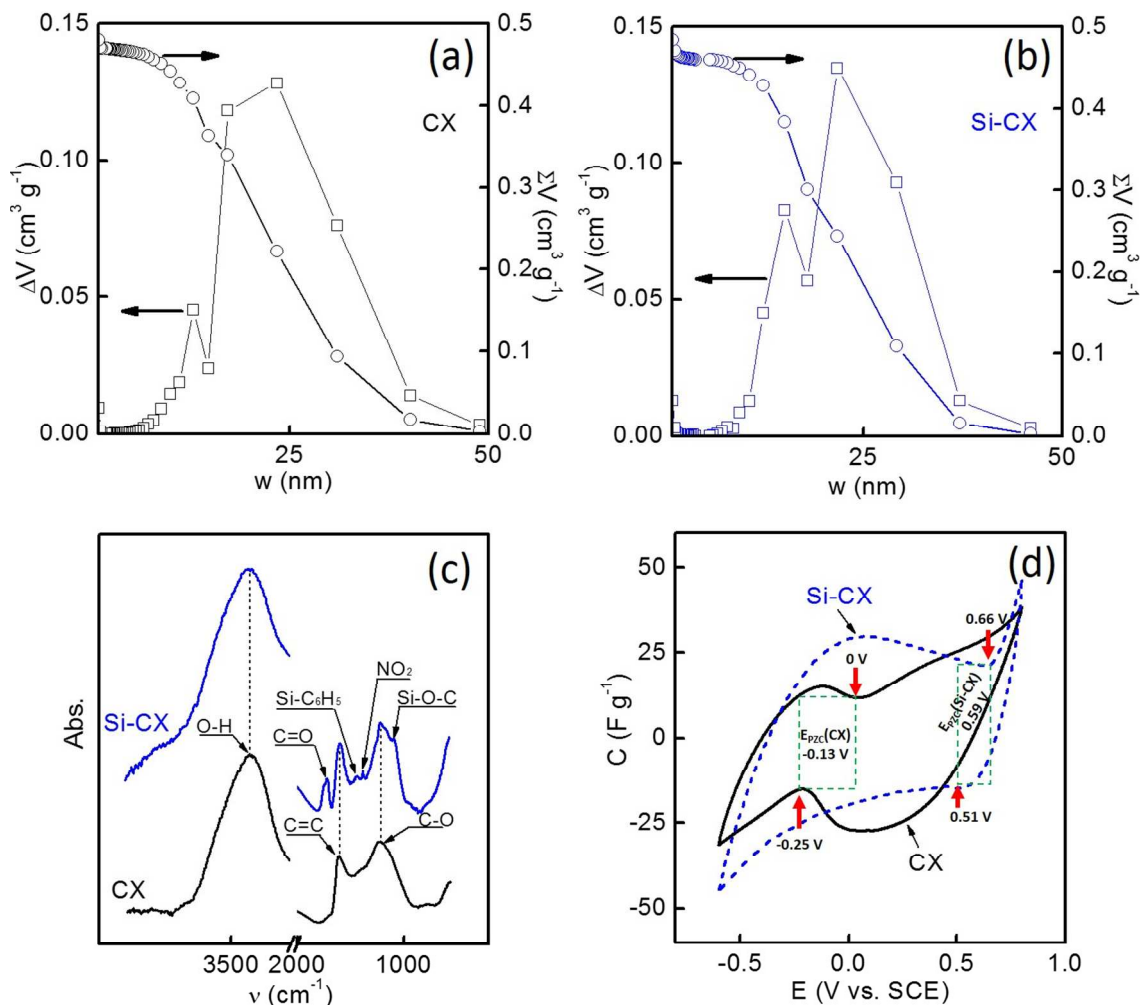


Figure 3. Characterization results for the CX and Si-CX electrodes. (a)-(b) The pore size distributions were quantified by the Barrett-Joyner-Halenda (BJH) method as the CX and Si-CX materials are mainly composed of mesopores (Fig. S2). (c) FTIR spectra of CX and Si-CX materials. (d) Cyclic voltammograms at 1 mV s⁻¹ in 4.3 mM deaerated NaCl solution. The capacitance (C) was calculated *via* $C = j / \nu$, where j is the current density and ν is the voltage scan rate. The dashed rectangles and arrows indicate the locations of E_{PZCS} .

3. Results and Discussion

3.1. Characterizations of Electrode Materials for an i-CDI System

In order to obtain the separation behavior desired for ion adsorption-desorption in i-CDI systems, CX and Si-CX materials were selected due to their completely different E_{PZCS} (or state of net surface charges).⁶⁰ Their similarities and dissimilarities were characterized through studies in pore size distribution, surface chemistry, and cyclic voltammetry.

The CX and Si-CX materials tested in this study are mainly composed of mesopores and macropores, which are depicted by their characteristic N_2 adsorption-desorption isotherms shown in Fig. S2. The Barrett-Joyner-Halenda (BJH) method was used to analyze their pore size distributions (Fig. 3(a)-(b)) by plotting the incremental pore volume (ΔV) and the cumulative pore volume (ΣV) as a function of pore width (w).^{61, 62} In general, the trend and magnitude of the ΔV and ΣV values for the Si-CX material are very comparable to those for the CX material, which suggests that the pore structure of the Si-CX material as measured by gas adsorption-desorption has been maintained. Furthermore, the pore volume for both the CX and Si-CX electrodes is approximate $0.5 \text{ cm}^3 \text{ g}^{-1}$ by summation of the ΔV values or by looking at the highest ΣV value.

The use of TEOS mixtures to modify the CX electrode surface leads to changes in its surface chemistry, which can be leveraged in the i-CDI process to make an asymmetric cell with respect to surface charge.⁴ As shown in Fig. 3(c), FTIR spectroscopy was employed to examine the chemical species at the material surface. C-O, C=C, and O-H stretching groups exist at both the CX and Si-CX electrode surfaces, while new bands at ~ 1730 , ~ 1430 and $\sim 1100 \text{ cm}^{-1}$ associated with C=O, Si-C₆H₅, and Si-O-C

stretching groups, respectively, are further identified at the Si-CX surface.⁶³ This assignment indicates that the modification results not only in the formation of a thin silicon-containing layer but also in the attachment of –COOH functional groups to the carbon surface.⁶³ It is known that oxidized Si has a negative zeta potential in neutral solution, and –COO[–] from the hydrolysis of –COOH carries a negative charge.^{5, 9, 11, 64-66} It is also known that carbon suspensions with an oxide layer possess a negative zeta potential in neutral salt solutions.^{36, 67-77} As a result, it is expected that the thin layer formed at the Si-CX material surface will have a negative zeta potential, which facilitates cation adsorption in a neutral solution. This negative zeta potential affects ion adsorption properties in the diffuse layer, as reflected by a relocation of the E_{PZC} of the electrode via Eq. [3].

$$\zeta = k_1(\text{pH}_{PZC} - \text{pH}) = k_2(E - E_{PZC}) \quad [3]$$

Eq. [3] shows the relationship between the zeta potential (ζ), potential of zero charge (E_{PZC}), and point of zero charge (pH_{PZC}), where E represents the potential at an electrode, and k_1 and k_2 are both positive constants.^{47, 78 79} Following from Eq. [3], at fixed E and pH values, a decrease in the ζ and pH_{PZC} values leads to an increase in the E_{PZC} value. Results validating this relationship (*i.e.*, pH_{PZC} vs. E_{PZC}) have been shown using commercially available SC materials in the literature.⁴⁰ For example, by electrochemical oxidation of the SC material, the pH_{PZC} value decreases from 7.40 for the untreated sample to 3.21 for the oxidized sample whereas the E_{PZC} value increases correspondingly from 164 mV to 355 mV.⁴⁰ As a consequence, it is assumed that the E_{PZC} value for the Si-CX electrode should be greater than that for the CX electrode.

The E_{PZC} of an electrode can be measured in a dilute salt solution by various electrochemical methods, *e.g.*, immersion^{39, 80, 81}, chronoamperometry⁵⁵, cyclic voltammetry (at low scan rate)^{54, 82-84}, and electrochemical impedance spectroscopy (at low frequency)⁸⁵. As shown in Fig. 3(d), a distinct ‘V-shape’ region (highlighted by a dashed rectangle) is formed in the voltammograms. Bard and Faulkner concluded that the E_{PZC} exists at the potential of the ‘V-shape’ region.⁵² (Based upon the Gouy-Chapman-Stern model for the electrochemical double layer, the effect of a salt solution on the ‘V-shape’ region was experimentally studied, and the corresponding plots are shown in Fig. S3.) In this study, the E_{PZC} is estimated by averaging the electrode’s potential at the minimal capacitance value in the ‘V-shape’ region at the both cathodic and anodic branches in the voltammograms. For instance, the E_{PZC} for the pristine CX in Fig. 3(d) is approximate -0.13 V vs. SCE. By looking at the location of the ‘V-shape’ region in Fig. 3(d), it can be understood that the E_{PZC} value for the Si-CX electrode is greater than that for the CX electrode, which is consistent with the prediction from Eq. [3]. Together with the earlier surface chemistry characterization (Fig. 3(c)), it is understood that this shift of the E_{PZC} in the positive direction is attributed to an increase in the net negative charges at the CX surface. Overall, the relocation of the E_{PZC} for an electrode reflects changes in the surface charges of carbon electrodes. (Fig. S5 demonstrates that an increase in net negative charges at HNO₃-treated CX and SC surfaces leads to the ‘V-shape’ region being positively shifted and E_{PZC} value being greater. This study was characterized through FTIR spectroscopy, pH titration, and cyclic voltammetry.)

It is also found that the ‘V-shape’ regions associated with the anodic and cathodic branches deviate slightly, especially for the CX electrode. This deviation is due to the

relatively high resistance at the interface between the electrodes and the solution, and the dependence of the E_{PZC} measurement on transient conditions, leading to the need for lower voltage scan rates to obtain better resolution.⁸³ The effect of voltage scan rate on the ‘V-shape’ region in the voltammogram was also examined in Fig. S4 in the supplementary information.

The E_{PZC} of a carbon electrode can be recognized as a transition potential region where the electrode has a least capability for ion adsorption⁵², which depends on the material’s surface tension,⁵² the total salt concentration^{52, 55}, the porosity of carbon electrodes^{83, 86}, and the solution’s pH⁴⁸. Furthermore, a representation by Levi *et al.* indicates that when an applied potential positively (or negatively) exceeds the E_{PZC} , anion-adsorption (or cation-adsorption) correspondingly becomes significant.^{52, 53, 87} As a consequence, knowledge of the E_{PZC} of a carbon electrode becomes fundamentally important to the operation of a CDI cell.⁴⁴ Unlike other electrochemical technologies that use a flow cell such as a redox flow battery or a fuel cell,⁸⁸⁻⁹⁰ the lack of substantial electrochemically active redox species restricts the thermodynamic prediction (*i.e.*, the Nernst equation) of the working voltage window in a CDI cell. Nevertheless, in order to improve the desalination performance of a CDI cell, the location of the E_{PZC} for both the cathode and anode has to be managed with respect to their working voltage window.⁴⁴ (The working voltage window means the voltage difference between the distributed potential at each electrode and the short-circuit potential.)

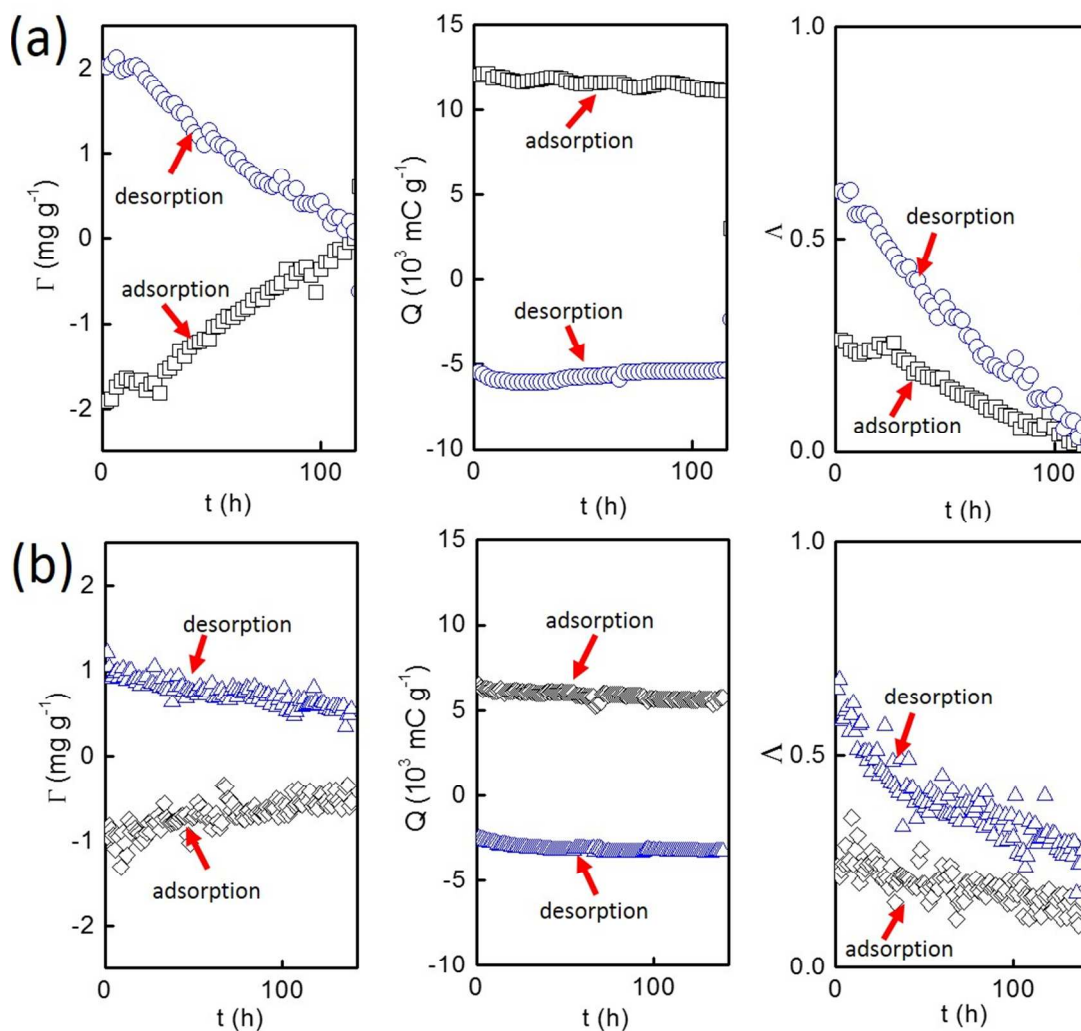


Figure 4. A plot of electroadsorption capacity (Γ), charge passed (Q), and charge efficiency (Δ) as a function of time (t) for a CDI cell operated at (a) 1.2/0 V and (b) 0.8/0 V in 31 L of 4.3 mM deaerated NaCl solution at 75 mL min^{-1} . In each study, 16 pairs of pristine CX electrodes were used as both the cathode and anode. Time taken for each half cycle for the tests at 1.2/0 and 0.8/0 V was 4000 and 2000 s, respectively, with the total operational hours being similar. The conductivity and current profiles can be found in Fig. S6 and S9.

3.2. Performance Degradation without E_{PZC} or Oxidation Management

Knowledge of the E_{PZC} location with respect to the electrode's working voltage window is critical to improving the electrosorption performance of a CDI cell.^{31, 33, 44, 45, 60} This earlier conclusion, drawn through long-term CDI operation, will be experimentally verified using CX electrodes in the following section and using commercially available ZX and SC electrodes in Fig. S7.

Cycling tests were performed using a CDI cell assembled with 16 pairs of pristine CX electrodes in 31 L of 4.3 mM deaerated NaCl solution at 75 mL min⁻¹. Based upon the full plot of conductivity and current profiles (Fig. S6 and S9), Fig. 4 shows the electrosorption capacity (Γ), charge passed (Q), and charge efficiency (Λ) for a CDI cell operated at (a) 1.2/0 V and (b) 0.8/0 V. Although these two tests were performed at different charging voltages for different charging periods during the adsorption step, a distinct similarity in performance exists. It is observed that in both cycling tests, the Γ values degrade with cycling but the corresponding Q values remain almost constant, resulting in the reduced Λ values. This observation is mainly attributed to changes in surface chemistry at the anode by electrochemical oxidation in an aqueous solution, resulting in the E_{PZC} being positively shifted. Evidence of anode oxidation can be found in earlier publications.^{11, 33} The E_{PZC} relocation is detailed in the following results on potential distribution measurements and cyclic voltammetry using a four-electrode setup. In addition, similar degradation performance is also observed in Fig. S7 when the commercially available ZX and SC electrodes were used in cycling tests.

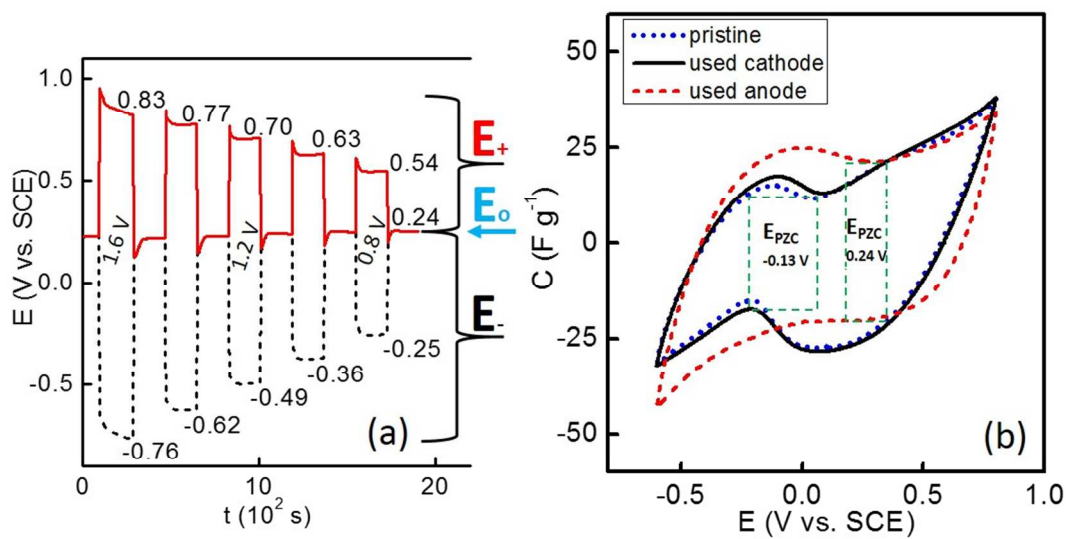


Figure 5. CX electrode characterizations from a four-electrode setup in 4.3 mM deaerated NaCl. (a) The potential distribution was measured at cell potentials between 0.8-1.6 V when a pair of pristine electrodes was used. Subsequently, 0.8 V was constantly applied to a pair of fresh electrodes for about 24 hours in the same solution to examine the E_{PZC} shift at a cell potential of 0.8 V. In turn, the resulting electrodes were examined by cyclic voltammetry at 1 mV s^{-1} . (b) In comparison to the E_{PZC} of the pristine CX electrode, the voltammograms show the E_{PZC} of the anode is relocated, while the E_{PZC} of the cathode is nearly maintained. In the plot, E_+ , E_- , and E_0 represent the potentials at the anode, cathode, and short-circuit, respectively.

3.3. Interpretation of Performance Degradation by E_{PZC} and Potential Distribution

The two working electrodes in the four-electrode setup were configured (similar to the CDI cell used in the cycling tests) to study potential distribution and E_{PZC} relocation in a simulated cell. Fig. 5(a) shows the potential distribution measured in 4.3 mM deaerated NaCl solution when a pair of pristine CX electrodes was used. Despite the unbalanced potential drops across the cathode and anode (the interpretation in detail can be found in our earlier publication³¹), even at 0.8 V applied from a power source, the distributed potential at the anode is greater than the thermodynamic potential for carbon oxidation in aqueous solution.^{33,36,91} Therefore, under these conditions, the anode surface is oxidized, which was confirmed by FTIR and XPS spectroscopy.^{11, 33} Correspondingly, negative surface charges are created on the carbon surface.

The voltammograms of Fig. 5(b) display that as compared to the pristine CX electrode, the ‘V-shape’ region for the used anode is apparently shifted in the positive direction while the ‘V-shape’ region for the used cathode is nearly maintained after using a cell potential of 0.8 V for 24 hours. Therefore, it can be understood that the E_{PZC} for the used anode has been positively shifted, which is due to an increase in net negative surface charges at the anode surface. This result is consistent with the positive shifting of the E_{PZC} for the Si-CX electrode depicted in Fig. 3(d).

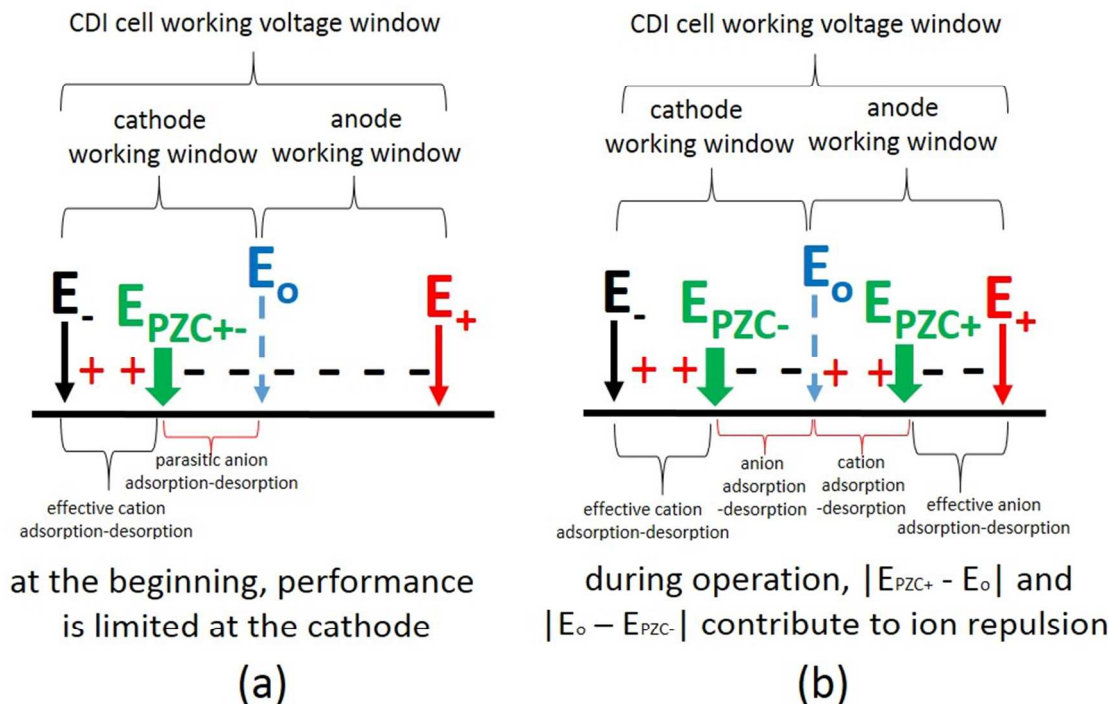


Figure 6. Based upon the measured potential distribution combined with the E_{PZC} relocation at the anode (Fig. 5), this schematic illustrates the mechanism for the performance degradation (Fig. 4). In this schematic, E_+ , E_- , and E_o represent the potentials at the anode, cathode, and short-circuit, respectively. E_{PZC+} and E_{PZC-} denote the E_{PZC} at the anode and cathode, respectively. It should be emphasized that when a potential at an electrode reaches the E_{PZC} , this electrode will have a least capability for ion adsorption. Furthermore, another representation of the effect of E_{PZC} location on the electrosorption performance can be found in publications by Cohen *et al.* and Avraham *et al.*^{33, 44}

When a CDI system is charged for ion adsorption, an applied voltage is naturally distributed to the cathode (E_-) and anode (E_+). When a CDI system is discharged at the short-circuit potential (E_o) for ion desorption, the distributed potentials at the cathode and anode are equivalent. Results for these variations in the potentials have been shown in Fig. 5(a) when a four-electrode setup was used. Based upon the measurements using a four-electrode setup, together with the mechanism developed by Avraham *et al.*,^{31, 44, 45} a schematic in Fig. 6 summarizes the effect of E_{PZC} relocation on CDI performance during long-term operation using CX materials (representative of the studied carbon electrodes). It can be seen in Fig. 6(a) that at the beginning, both E_{PZC} s for the pristine electrodes are located in the cathodic working window (*i.e.*, $|E_o - E_-|$), which means that a part of the working voltage (*i.e.*, $|E_{PZC-} - E_o|$) at the cathode is consumed by parasitic anion adsorption-desorption. For example, according to Fig. 5(a), when 1.2 V is applied to the cell from a power source, the $E_{PZC} \approx -0.13$ V falls between $E_o \approx 0.24$ V and $E_- \approx -0.49$ V. Therefore, only 0.36 V (*i.e.*, $|E_{PZC-} - E_-|$) is used to adsorb cations at the cathode rather than 0.73 V (*i.e.*, $|E_o - E_-|$). This loss in the effective working voltage for cation adsorption is interpreted by the presence of native net positive charges at the surface of the pristine electrode, correspondingly resulting in the location of the E_{PZC} in the cathodic working voltage window. Under such anion adsorption-desorption conditions, H_2O molecules are dissociated to maintain electroneutrality in the cell. Therefore, as reported in another study, pH of the NaCl solution at the outlet of the CDI cell is functionally changed but without a dramatic impact on conductivity.^{31, 33, 34, 92, 93}

With continued operation shown in Fig. 6(b), the E_{PZC} for the cathode (E_{PZC-}) is almost stationary. However, the E_{PZC} for the anode (E_{PZC+}) is shifted into the anodic

working window with the addition of an oxide layer at the anode.³¹ Consequently, the working voltage created (*i.e.*, $|E_{PZC+} - E_0|$) for cation adsorption-desorption paired with the present working voltage (*i.e.*, $|E_{PZC-} - E_0|$) for anion adsorption-desorption contributes to a reduction in the net salt removal capacity, which can be observed (in Fig. 9(a), S6-7, and S9) by looking at the ion repulsion peaks at the beginning of each adsorption step in the CDI cells. In Fig. S8, we also depict the degradation mechanism when the electrode's polarity is reversed.

The schematic in Fig. 6 also suggests that in order to maintain desalination performance in CDI systems, the E_{PZC} associated with the anode has to be managed or fixed in one place with respect to its working voltage window. Since we have demonstrated that E_{PZC} shifting is caused by carbon oxidation in aqueous solution, the development of anode materials with good oxidation resistance for CDI applications should be a paramount research direction.³³ However, without such materials, an alternative route would be to make use of the native surface charges created in the CDI cell to aid in the separation process. Thus, together with the degradation mechanism (Fig. 6(b)), the repulsion peaks observed during the adsorption step (Fig. 9(a), S6-7, and S9) prompted us to exploit carbon electrodes with dissimilar surface charge states for CDI applications.

3.4. Inverted Capacitive Deionization (i-CDI)

Recent studies have shown that the desalination performance of a CDI cell degraded during cycling tests, which is due to the relocation of the E_{PZC} at the anode, in turn disrupting the potential distribution.³¹⁻³⁴ In order to enhance the stability of CDI

operation, the degree of E_{PZC} shifting at the anode has to be minimized. As shown earlier in Fig. 4, one method could be the use of a smaller applied voltage to charge a CDI cell, resulting in slower degradation at 0.8/0 V compared to that at 1.2/0 V. This slower degradation is attributed to the smaller potential distributed at the anode, which reduces oxidation of the anode in an aqueous solution. Another alternative would be the use of a constant-current charging method, which limits the charging time spent at substantial oxidizing potentials.^{5, 94} However, in order to improve the electrosorption capacity and charge efficiency of a CDI cell, the applied voltage should be as high as possible based upon the GCS model for CDI applications.²⁶ In order to overcome these difficulties, a novel system, called inverted capacitive deionization (i-CDI), has been developed to achieve both stable and efficient desalination performance.

The i-CDI working principle in Fig. 7(a) and 1(b) shows that by using a CDI cell with asymmetric electrodes, the voltage window between the two E_{PZCS} can be used for the adsorption-desorption process. This is opposed to the potential window outside of these E_{PZCS} , which has been classically used. In this new i-CDI case, unlike the CDI system, further oxidation of the anode would not have a detrimental effect on the salt separation performance. In fact, the oxygen-containing functional groups from oxidation would increase the net negative surface charges, further expanding the internal working voltage window for desalination for the i-CDI systems, where the E_{PZCS} at the cathode (E_{PZC-}) and anode (E_{PZC+}) are diametrically opposed with respect to the short-circuit voltage (E_0).

Under such an electrode configuration, when an applied voltage is smaller than the difference between the two E_{PZCS} (*i.e.*, $|E_{PZC+} - E_{PZC-}|$), the adsorption-desorption

performance is completely inverted. In detail, when the potential at the cathode (E_-) and anode (E_+) approach the E_{PZC-} and E_{PZC+} under a charging condition, anions and cations are desorbed as ion adsorption at the E_{PZC} for an electrode has a minimum capacitance value.^{53, 54} When the cathode and anode are shorted under a discharging condition, anions and cations are adsorbed as ion adsorption becomes significant far beyond the E_{PZC} .^{53, 54} The feasibility and merits of the i-CDI operation will be demonstrated in the following paragraphs.

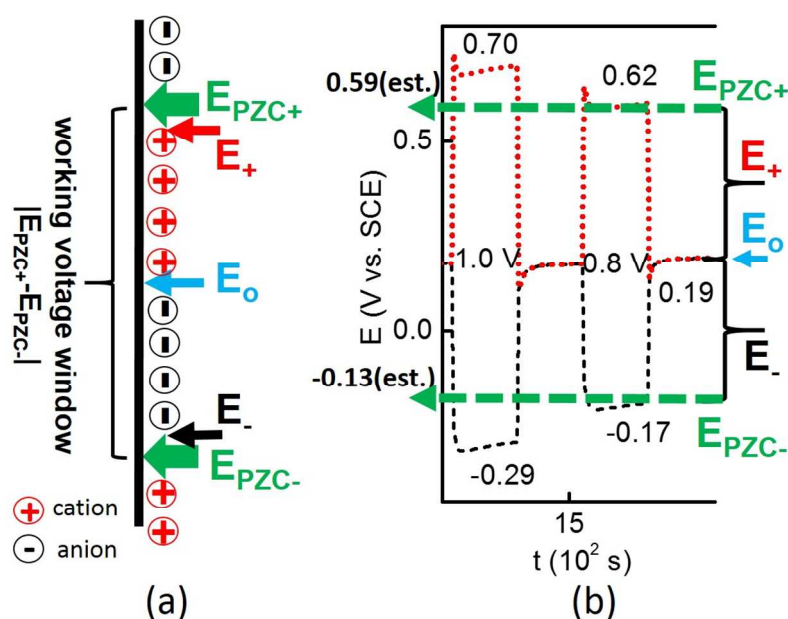


Figure 7. (a) A novel CDI system is proposed, named inverted capacitive deionization (i-CDI). When the E_{PZC} s for both electrodes are dissimilarly located with respect to the short-circuit voltage (E_0), the potential window between the E_{PZC} s at the anode and cathode can be used for the desalination process, but the adsorption-desorption behavior will be totally inverted. (b) Potentials distributed at the anode (E_+) and cathode (E_-) at a total cell potential of 0.8 and 1 V in 4.3 mM deaerated NaCl solution when a Si-CX anode and pristine CX cathode were used in a four-electrode cell.

In order to create the voltage window depicted in Fig. 7(a), electrodes with opposing E_{PZC} s needed to be introduced. According to the effect of oxides at the electrode surface on E_{PZC} shifting, for i-CDI applications, the surface of the anode needs to contain a native net negative charge (*i.e.*, Si-CX material in this example) and the opposing cathode needs to have a native net positive charge (*i.e.*, pristine CX material in this example).

Since the same configuration (*i.e.*, solution concentration and electrode spacing) was used in both the four-electrode and flow-through cells, the E_{PZC} and potential distribution measurements are suited for the CX and Si-CX electrodes used in an i-CDI system. As reported earlier in Fig. 3(d) of the voltammograms, the ‘V-shape’ region in the voltammogram for the CX and Si-CX materials is approximately placed at $-0.25 - 0$ V and $0.51 - 0.66$ V *vs.* SCE, respectively. By averaging the location of the ‘V-shape’ regions, the E_{PZC} for the CX and Si-CX electrodes is approximately -0.13 and 0.59 V *vs.* SCE, respectively. Therefore, it can be estimated that an approximate potential of 0.72 V under a charging condition could be used for salt desorption in the i-CDI system.

To screen the utilization of all of the estimated voltage, the potentials distributed at the Si-CX anode (E_+) and CX cathode (E_-) need to be examined in 4.3 mM deaerated NaCl solution. As shown in Fig. 7(b), with 0.8 V applied by a power source, the potentials distributed at the Si-CX anode (E_+) and CX cathode (E_-) have values of ~ 0.62 and ~ -0.17 V *vs.* SCE, respectively, where the short-circuit voltage (E_o) is ~ -0.19 V *vs.* SCE. By comparing the E_{PZC} values to the potential distribution plot, we assume that the maximum applied voltage for the i-CDI cell using these electrodes should be 0.8 ± 0.1 V, and a more precise applied voltage should be studied using a flow-through system. For

this study, a suitable voltage for the i-CDI system is 0.8 V (see the counterproductive effect at 0.9 V in Fig. S13), which is slightly greater than the estimated value by the E_{PZC} locations but within the range of the measured E_{PZC} values.

3.5. Initial Desalination Performance Using i-CDI and CDI Systems

i-CDI cycling tests were performed at 0.8/0 V in 4.3 mM deaerated NaCl solution at 75 mL min⁻¹. Under the same conditions, a parallel study was carried out using a CDI system for comparison. Fig. 8 shows conductivity and current for 3 cycles during initial testing. Clearly, the use of the i-CDI system results in the adsorption and desorption performance being completely inverted compared to the use of the CDI system, where salt desorption occurs during the charging step at 0.8 V, and salt adsorption occurs during the discharging step at short-circuit voltage. Furthermore, the i-CDI method offers more resolved salt separation and considerably less current at steady state during charging. As a result, the charge efficiency calculated according to Eq. [1] and [2] is correspondingly enhanced to ~50% for the charging step and ~80% for the discharging step which is substantially higher than ~25% and ~55% associated with the CDI cell. This improvement in the salt separation can be attributed to the use of a new working voltage window, where performance is less affected by the location of the respective E_{PZC} areas of the electrodes by eliminating potentials in excess of the respective E_{PZCS} .^{44, 45} The reduction in current at steady state is partially attributed to the lack of substantial oxidation of the Si-CX anode since an oxide layer has already been formed at this electrode.

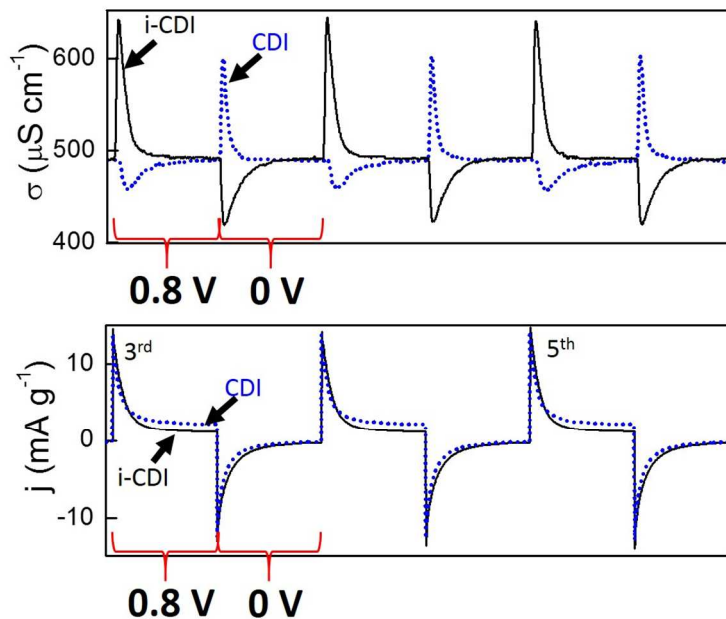


Figure 8. Selected profiles of the conductivity (σ) and current density (j) during initial cycling (3rd-5th) for i-CDI and CDI systems at 0.8/0 V in 31 L of 4.3 mM deaerated NaCl solution at 75 mL min⁻¹. The full plots can be found in Fig. S9 and S12.

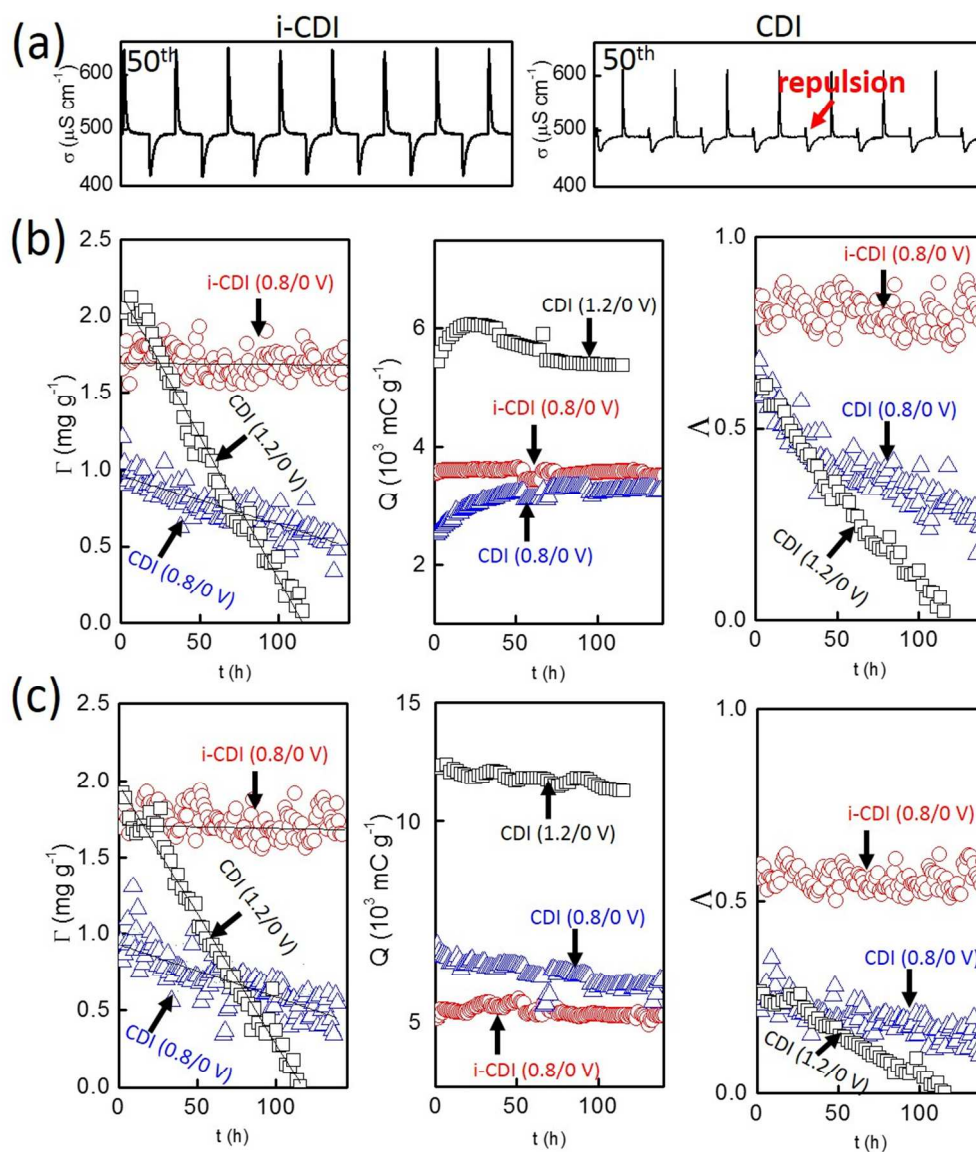


Figure 9. (a) Selected profiles of the conductivity (σ) at the 50-57th cycles for i-CDI and CDI systems at 0.8/0 V in 31 L of 4.3 mM deaerated NaCl solution at 75 mL min⁻¹. Based on the data for (b) discharging at 0 V and (c) charging at 0.8 V, the electrosorption capacity (Γ), charge passed (Q), and charge efficiency (Λ) were evaluated. Due to inverted salt adsorption-desorption behavior for the i-CDI system, the absolute values of Γ and Q were used to calculate the Λ value. In addition, data for the CDI system used at 1.2/0 V was added into the plots for comparison.

3.6. Performance Stability using i-CDI and CDI Systems

Fig. 9(a) shows the salt separation performance for cells using the i-CDI and CDI systems during long-term operation. Compared to the performance at the initial stage shown in Fig. 8, salt separation using the i-CDI system has been remarkably well maintained. In contrast, salt separation using the CDI system shows repulsion (or desorption) peaks at the beginning of each adsorption step (*i.e.*, after the voltage was switched on), resulting in the salt separation being degraded. This repulsion spike can thus be recognized as an indicator of performance degradation during CDI operation (also observed in Fig. S7 for CDI cells formed with commercially available ZX and SC materials as the electrodes.).

More evidence demonstrating the higher stability and efficiency of the i-CDI system has been summarized in Fig. 9(b)-(c) using the electrosorption capacity (Γ), charge passed (Q), and charge efficiency (Λ) as metrics. It can be seen that under the same experimental conditions, the Γ values of $\sim 1.7 \text{ mg g}^{-1}$ for the i-CDI system are nearly constant over the entire testing period, whereas the Γ values for the CDI system decayed from its highest capacity of $\sim 1 \text{ mg g}^{-1}$, decreasing to $\sim 0.5 \text{ mg g}^{-1}$. Salt separation performance of the i-CDI system is better than the initial performance for the CDI system and much better during long-term examination. At 0.8 V under a charging condition, the Q values for the i-CDI system are smaller than that for the CDI system, indicating that less energy is required in the overall separation process using this inverted behavior. During operation at the short-circuit voltage, the Q values for the i-CDI system are slightly greater than those for the CDI system. By Eq. [1]-[2], the Λ values for the i-CDI system are always greater than that for the CDI system in both the charging and

discharging steps. In addition, by comparing the performance data for the CDI system operated at 1.2/0 V vs. 0.8/0 V, it is evident that the use of higher voltage at the adsorption step hastens performance degradation in standard CDI systems.

In contrast to the conventional CDI system, improvement in the charge efficiency of the i-CDI system is attributed to the use of a new working voltage window, avoiding interference with the E_{PZCS} of each electrode.^{44, 45} Furthermore, the inverted behavior is due to the use of dissimilarly surface charged electrodes. Therefore, ion adsorption is mainly due to the native electrostatic force generated by a spontaneously formed EDL at a chemically-modified surface of a carbon electrode. However, ion desorption requires an external power source for the i-CDI system.

i-CDI system testing was subsequently repeated with the same electrode configuration (*i.e.*, CX cathode and Si-CX anode) for over 600 hours of operation. Fig. 10 shows the excellent stability compared to those by conventional CDI systems. For example, the time taken for the 1.2/0 V operated CDI cell to completely lose salt separation capability was ~100 hours, while stable salt separation for 0.8/0 V operation in the i-CDI cell was maintained for the testing period of ~630 hours. As a result, an increase of at least ~530% in lifetime was achieved in comparison to the 1.2/0 V operated CDI cell with comparable initial performance. (The conductivity and current profiles are shown in Fig. S14.)

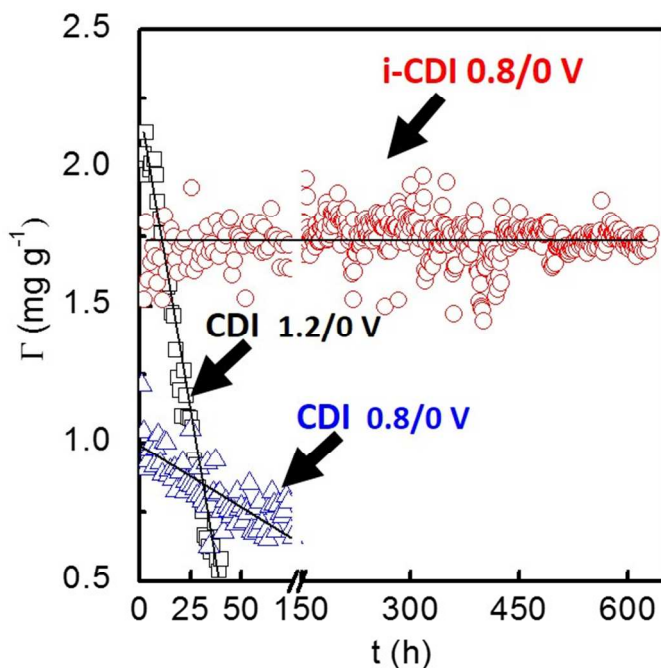


Figure 10. Enhanced stability by the i-CDI system employed with a CX cathode and a Si-CX anode. This test was performed at 0.8/0 V in 31 L of 4.3 mM deaerated NaCl solution. The full plots can be found in Fig. S14. Comparisons in performance to standard CDI operation under similar conditions with pristine CX electrodes are shown. In this plot, lines have been added to guide the eyes.

Overall, the i-CDI system shows no performance degradation over the time tested. This increased stability during long-term operation is accounted for by the managed surface chemistry and corresponding placement of the E_{PZCS} for the electrodes. This is exemplified in Fig. 11 by comparing the voltammograms for each electrode before and after cycling. (The cell was disassembled, and the cycled electrodes were resized for voltammetric characterization.) It is found that the ‘V-shape’ regions for the cycled

electrodes are only slightly shifted compared to that for the initial electrodes, indicating that the location of the E_{PZC} of the anode and cathode has been maintained.

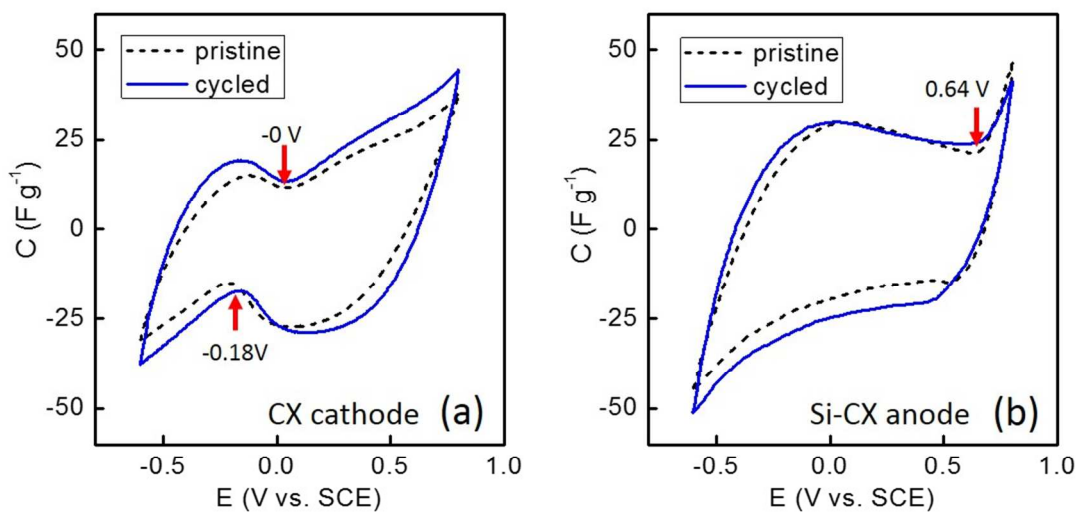


Figure 11. After the cycling tests using the i-CDI system shown in Fig. 8-9, the cycled electrodes were resized and electrochemically characterized at 1 mV s^{-1} in 4.3 mM deaerated NaCl solution. The voltammograms for the cycled (a) CX and (b) Si-CX electrodes. The voltammograms for the pristine CX and Si-CX electrodes are correspondingly overlaid.

3.7. Future Works and Outlook

The developed i-CDI system is currently limited by the use of a relatively small voltage window, approximately 0.8 V for this study, due to the extent of shift in the E_{PZCS} achieved (In the supplementary information, Fig. S13 shows that i-CDI performance was reduced at $0.9/0 \text{ V}$ operation.). Therefore, we suggest that future studies examine the electrosorption capacity and charge efficiency of carbon electrodes with either more

positive or negative E_{PZC} s to further expand the internal working voltage window for i-CDI applications. For instance, according to Eq. [3], the E_{PZC} location can be further positively shifted if the coated nanomaterials have a more negative ζ -potential. Furthermore, the use of this method combined with the development of carbon materials with much higher pore volume (*e.g.*, carbon aerogel via supercritical drying or thermally activated carbon electrodes⁶²) may aid in increasing stable and high-capacity salt separation performance. In addition, since we have demonstrated the influence of surface chemistry and the E_{PZC} location on salt separation performance, if the E_{PZC} of the respective carbon electrodes could be measured in situ, CDI may be further optimized to avoid degradation pathways.

Beyond the development of the i-CDI system, the use of a constant-current charging method may be feasible in minimizing oxidation at the anode for a sustainable conventional CDI process. This is because when a constant-current is applied to a CDI cell, the measured cell voltage increases slowly up to a desired cutoff voltage,^{5, 94} which minimizes the oxidation rate at the anode. In contrast, when a constant-voltage is applied to a CDI cell, the measured cell voltage almost immediately jumps to the applied voltage,^{29, 94} which accelerates the oxidation rate at the anode's surface during the charging cycle.

Finally, we consider that a plot of the E_{PZC} with respect to the potential distribution can be used for model development. For instance, in Fig. 7(b) and S15, it is found that the applied voltage was almost equally distributed to each electrode when the pristine and Si-CX materials were used as cathodes and anodes, respectively. This result

suggests that in addition to the E_{PZC} , a model developed by Zhao *et al.*²⁶ (and summarized by Porada *et al.*⁵) could be used to predict desalination performance for an i-CDI system.

4. Conclusions

Through long-term operation of a CDI system operated at constant voltage, performance degradation was observed with conventional symmetric pristine carbon electrodes. For instance, a CDI system operated at 1.2/0 V completely lost salt separation capacity after ~100 hours of operation. This degradation in performance is mainly attributed to the relocation of the E_{PZC} at the anode by electrochemical oxidation resulting in changes in surface chemistry (*e.g.*, carboxylic groups) at the anode surface. In order to improve the performance stability, we developed a new system called inverted capacitive deionization (i-CDI) where ion adsorption and desorption occurs in phases opposed to the conventional concept of the CDI working principle where reducing the cell voltage leads to ion desorption.

The i-CDI system was demonstrated via the use of CX with a negative E_{PZC} (or net positive charges at the surface) and Si-CX with a positive E_{PZC} (or net negative charges at the surface) as the cathode and anode, respectively. Long-term cycling results showed that i-CDI performance was maintained for over 600 hours, which is an increase of ~530% in lifetime in comparison to a CDI cell operated at 1.2/0 V. This significant enhancement in cycling stability is attributed to the use of a Si-CX anode with net negative surface charges and a more positive E_{PZC} value. In turn, further electrochemical oxidation at this anode only increases the enhancement in net negative surface charges, which correspondingly facilitates the E_{PZC} being more positively shifted and expands the

working voltage window for the i-CDI system. Overall salt capacity of the cell remained somewhat limited due to the small working voltage window between the E_{PZCS} , but future studies aim to further extend this voltage window.

Acknowledgements

The authors are grateful to the U.S. - China Clean Energy Research Center, U.S. Department of Energy for project funding (No. DE-PI0000017). The authors would also like to thank Dr. R. Frimpong, Dr. N. Holubowitch, Dr. L. Widger, and Mr. J. Rentschler for their useful discussions, and Mr. R. Perrone for help in designing and constructing the CDI cells.

References

1. S. J. Montain, W. A. Latzka and M. N. Sawka, *Military Medicine*, 1999, **164**, 502-508.
2. <http://water.epa.gov/scitech/swguidance/standards/handbook/chapter03.cfm>. (last access: 07-Jan-2015)
3. <http://www.lakesidewater.com/index.html>. (last access: 07-Jan-2015)
4. M. A. Anderson, A. L. Cudero and J. Palma, *Electrochim. Acta*, 2010, **55**, 3845-3856.
5. S. Porada, R. Zhao, A. van der Wal, V. Presser and P. M. Biesheuvel, *Prog. Mater. Sci.*, 2013, **58**, 1388-1442.
6. Y. Oren, *Desalination*, 2008, **228**, 10-29.
7. H. Li, F. Zaviska, S. Liang, J. Li, L. He and H. Y. Yang, *J. Mater. Chem. A*, 2014, **2**, 3484-3491.
8. C. Tsouris, R. Mayes, J. Kiggans, K. Sharma, S. Yiacoumi, D. DePaoli and S. Dai, *Environ. Sci. Technol.*, 2011, **45**, 10243-10249.
9. J. J. Wouters, J. J. Lado, M. I. Tejedor-Tejedor, R. Perez-Roa and M. A. Anderson, *Electrochim. Acta*, 2013, **112**, 763-773.

10. L. Wang, M. Wang, Z.-H. Huang, T. Cui, X. Gui, F. Kang, K. Wang and D. Wu, *J. Mater. Chem.*, 2011, **21**, 18295-18299.
11. X. Gao, J. Landon, J. K. Neathery and K. Liu, *J. Electrochem. Soc.*, 2013, **160**, E106-E112.
12. D. Zhang, X. Wen, L. Shi, T. Yan and J. Zhang, *Nanoscale*, 2012, **4**, 5440-5446.
13. B. Jia and L. Zou, *Chem. Phys. Lett.*, 2012, **548**, 23-28.
14. K. Laxman, M. T. Z. Myint, H. Bourdouceu and J. Dutta, *ACS Appl. Mater. Interfaces*, 2014, **6**, 10113-10120.
15. Q. Wang, J. Yan, Y. Wang, T. Wei, M. Zhang, X. Jing and Z. Fan, *Carbon*, 2014, **67**, 119-127.
16. J. C. Farmer, D. V. Fix, G. V. Mack, R. W. Pekala and J. F. Poco, *J. Electrochem. Soc.*, 1996, **143**, 159-169.
17. J. C. Farmer, D. V. Fix, G. V. Mack, R. W. Pekala and J. F. Poco, *J. Appl. Electrochem.*, 1996, **26**, 1007-1018.
18. I. Villar, S. Roldan, V. Ruiz, M. Granda, C. Blanco, R. Menéndez and R. Santamaría, *Energy Fuels*, 2010, **24**, 3329-3333.
19. H. Li, L. Zou, L. Pan and Z. Sun, *Environ. Sci. Technol.*, 2010, **44**, 8692-8697.
20. J. J. Lado, J. J. Wouters, M. I. Tejedor-Tejedor, M. A. Anderson and E. García-Calvo, *J. Electrochem. Soc.*, 2013, **160**, E71-E78.
21. S.-i. Jeon, H.-r. Park, J.-g. Yeo, S. Yang, C. H. Cho, M. H. Han and D. K. Kim, *Energy Environ. Sci.*, 2013, **6**, 1471-1475.
22. S. Porada, D. Weingarth, H. V. M. Hamelers, M. Bryjak, V. Presser and P. M. Biesheuvel, *J. Mater. Chem. A*, 2014, **2**, 9313-9321.
23. Y. Gendel, A. K. E. Rommerskirchen, O. David and M. Wessling, *Electrochem. Commun.*, 2014, **46**, 152-156.
24. K. B. Hatzell, E. Iwama, A. Ferris, B. Daffos, K. Urita, T. Tzedakis, F. Chauvet, P.-L. Taberna, Y. Gogotsi and P. Simon, *Electrochem. Commun.*, 2014, **43**, 18-21.
25. J. Lee, S. Kim, C. Kim and J. Yoon, *Energy Environ. Sci.*, 2014, **7**, 3683-3689.
26. R. Zhao, P. M. Biesheuvel, H. Miedema, H. Bruning and A. van der Wal, *J. Phys. Chem. Lett.*, 2010, **1**, 205-210.
27. P. M. Biesheuvel, S. Porada, M. Levi and M. Z. Bazant, *J. Solid State Electrochem.*, 2014, **18**, 1365-1376.
28. C. A. R. Perez, O. N. Demirel, R. L. Clifton, R. M. Naylor and C. H. Hidrovo, *J. Electrochem. Soc.*, 2013, **160**, E13-E21.
29. M. E. Suss, T. F. Baumann, W. L. Bourcier, C. M. Spadaccini, K. A. Rose, J. G. Santiago and M. Stadermann, *Energy Environ. Sci.*, 2012, **5**, 9511-9519.
30. T. J. Welgemoed and C. F. Schutte, *Desalination*, 2005, **183**, 327-340.

31. X. Gao, A. Omosebi, J. Landon and K. Liu, *J. Electrochem. Soc.*, 2014, **161**, E159-E166.
32. A. Omosebi, X. Gao, J. Landon and K. Liu, *ACS Appl. Mater. Interfaces.*, 2014, **6**, 12640-12649.
33. I. Cohen, E. Avraham, Y. Bouhadana, A. Soffer and D. Aurbach, *Electrochim. Acta*, 2013, **106**, 91-100.
34. Y. Bouhadana, E. Avraham, M. Noked, M. Ben-Tzion, A. Soffer and D. Aurbach, *J. Phys. Chem. C*, 2011, **115**, 16567-16573.
35. E. Ayranci and B. E. Conway, *J. Appl. Electrochem.*, 2001, **31**, 257-266.
36. K. Kinoshita, *Carbon - Electrochemical and Physicochemical Properties*, John Wiley & Sons, New York, 1988.
37. A. D. Jannakoudakis, P. D. Jannakoudakis, E. Theodoridou and J. O. Besenhard, *J. Appl. Electrochem.*, 1990, **20**, 619-624.
38. J. S. Noh and J. A. Schwarz, *J. Colloid Interface Sci.*, 1989, **130**, 157-164.
39. H. Tobias and A. Soffer, *J. Electroanal. Chem. Interfacial Electrochem.*, 1983, **148**, 221-232.
40. E. Bayram and E. Ayranci, *Electrochim. Acta*, 2011, **56**, 2184-2189.
41. E. Bayram and E. Ayranci, *Carbon*, 2010, **48**, 1718-1730.
42. P. M. Biesheuvel, Y. Fu and M. Z. Bazant, *Russ. J. Electrochem.*, 2012, **48**, 580-592.
43. E. Avraham, M. Noked, Y. Bouhadana, A. Soffer and D. Aurbach, *Electrochim. Acta*, 2010, **56**, 441-447.
44. E. Avraham, M. Noked, I. Cohen, A. Soffer and D. Aurbach, *J. Electrochem. Soc.*, 2011, **158**, P168-P173.
45. I. Cohen, E. Avraham, M. Noked, A. Soffer and D. Aurbach, *J. Phys. Chem. C*, 2011, **115**, 19856-19863.
46. Y. Oren, H. Tobias and A. Soffer, *J. Electroanal. Chem. Interfacial Electrochem.*, 1984, **162**, 87-99.
47. E. McCafferty, *Electrochim. Acta*, 2010, **55**, 1630-1637.
48. M. C. Hatzell, M. Raju, V. J. Watson, A. G. Stack, A. C. T. van Duin and B. E. Logan, *Environ. Sci. Technol.*, 2014, **48**, 14041-14048.
49. R. Zhang, L. Wolters and J. W. Weidner, *Int. J. Hydrogen Energy*, 2012, **37**, 2935-2939.
50. J. Wang, G. Yin, Y. Shao, S. Zhang, Z. Wang and Y. Gao, *J. Power Sources*, 2007, **171**, 331-339.
51. S. Zhang, X.-Z. Yuan, J. N. C. Hin, H. Wang, K. A. Friedrich and M. Schulze, *J. Power Sources*, 2009, **194**, 588-600.

52. A. J. Bard and L. R. Faulkner, *Electrochemical Methods - Fundamentals and Applications*, John Wiley & Sons, New York, 2001.
53. M. D. Levi, S. Sigalov, D. Aurbach and L. Daikhin, *J. Phys. Chem. C*, 2013, **117**, 14876-14889.
54. M. D. Levi, S. Sigalov, G. Salitra, R. Elazari and D. Aurbach, *J. Phys. Chem. Lett.*, 2011, **2**, 120-124.
55. D. C. Grahame, *Chem. Rev.*, 1947, **41**, 441-501.
56. A. N. Frumkin, O. A. Petrii and B. B. Damaskin, in *Comprehensive Treatise of Electrochemistry*, eds. J. O. M. Bockris, B. Conway and E. Yeager, Springer US, 1980.
57. M. Marino, L. Misuri, M. L. Jiménez, S. Ahualli, O. Kozynchenko, S. Tennison, M. Bryjak and D. Brogioli, *J. Colloid Interface Sci.*, 2014, **436**, 146-153.
58. J. C. Lytle, J. M. Wallace, M. B. Sassin, A. J. Barrow, J. W. Long, J. L. Dysart, C. H. Renninger, M. P. Saunders, N. L. Brandell and D. R. Rolison, *Energy Environ. Sci.*, 2011, **4**, 1913-1925.
59. J. Landon, X. Gao, B. Kulengowski, J. K. Neathery and K. Liu, *J. Electrochem. Soc.*, 2012, **159**, A1861-A1866.
60. X. Gao, A. Omosebi, J. Landon and K. Liu, *Electrochem. Commun.*, 2014, **39**, 22-25.
61. P. A. Webb, C. Orr, R. W. Camp, J. P. Olivier and Y. S. Yunes, *Analytical Methods in Fine Particle Technology*, Micromeritics Instrument, 1997.
62. T. F. Baumann, M. A. Worsley, T. Y.-J. Han and J. H. Satcher Jr, *J. Non-Cryst. Solids*, 2008, **354**, 3513-3515.
63. B. Stuart, *Infrared Spectroscopy: Fundamentals and Applications*, Wiley, 2004.
64. J. J. Wouters, J. J. Lado, M. I. Tejedor-Tejedor and M. A. Anderson, *J. Electrochem. Soc.*, 2012, **159**, A1374-A1382.
65. K. C. Leonard, J. R. Genthe, J. L. Sanfilippo, W. A. Zeltner and M. A. Anderson, *Electrochim. Acta*, 2009, **54**, 5286-5291.
66. J. J. Lado, R. E. Pérez-Roa, J. J. Wouters, M. Isabel Tejedor-Tejedor and M. A. Anderson, *Sep. Purif. Technol.*, 2014, **133**, 236-245.
67. V. Strelko Jr, D. J. Malik and M. Streat, *Carbon*, 2002, **40**, 95-104.
68. P. Chingombe, B. Saha and R. J. Wakeman, *Carbon*, 2005, **43**, 3132-3143.
69. D. J. Malik, V. Strelko Jr, M. Streat and A. M. Puziy, *Water Res.*, 2002, **36**, 1527-1538.
70. V. Strelko Jr and D. J. Malik, *J. Colloid Interface Sci.*, 2002, **250**, 213-220.
71. J. Binner and Y. Zhang, *J. Mater. Sci. Lett.*, 2001, **20**, 123-126.
72. A. B. García, A. Cuesta, M. A. Montes-Morán, A. Martínez-Alonso and J. M. D. Tascón, *J. Colloid Interface Sci.*, 1997, **192**, 363-367.

73. H. Hu, A. Yu, E. Kim, B. Zhao, M. E. Itkis, E. Bekyarova and R. C. Haddon, *J. Phys. Chem. B*, 2005, **109**, 11520-11524.
74. L. Vaisman, G. Marom and H. D. Wagner, *Adv. Funct. Mater.*, 2006, **16**, 357-363.
75. A. Schierz and H. Zänker, *Environ. Pollut.*, 2009, **157**, 1088-1094.
76. J. Lee, E.-J. Park, J. Choi, J. Hong, and S.-E. Shim, *Synth. Met.*, 2010, **160**, 566.
77. Y. Si and E. T. Samulski, *Nano Lett.*, 2008, **8**, 1679-1682.
78. P. H. Tewari and A. B. Campbell, *J. Colloid Interface Sci.*, 1976, **55**, 531-539.
79. P. H. Tewari and A. W. McLean, *J. Colloid Interface Sci.*, 1972, **40**, 267-272.
80. G. J. Clark, T. N. Andersen, R. S. Valentine and H. Eyring, *J. Electrochem. Soc.*, 1974, **121**, 618-622.
81. S. H. Kim, *J. Phys. Chem.*, 1973, **77**, 2787-2789.
82. C.-H. Hou, C. Liang, S. Yiacoumi, S. Dai and C. Tsouris, *J. Colloid Interface Sci.*, 2006, **302**, 54-61.
83. K.-L. Yang, S. Yiacoumi and C. Tsouris, *J. Electroanal. Chem.*, 2003, **540**, 159-167.
84. M. Hahn, M. Baertschi, O. Barbieri, J.-C. Sauter, R. Kötz and R. Gally, *Electrochem. Solid-State Lett.*, 2004, **7**, A33-A36.
85. L.-H. Shao, J. Biener, D. Kramer, R. N. Viswanath, T. F. Baumann, A. V. Hamza and J. Weissmuller, *Phys. Chem. Chem. Phys.*, 2010, **12**, 7580-7587.
86. R. K. Kalluri, M. M. Biener, M. E. Suss, M. D. Merrill, M. Stadermann, J. G. Santiago, T. F. Baumann, J. Biener and A. Striolo, *Phys. Chem. Chem. Phys.*, 2013, **15**, 2309-2320.
87. S. Srinivasan, in *Fuel Cells*, Springer US, 2006.
88. M. Skyllas-Kazacos, M. H. Chakrabarti, S. A. Hajimolana, F. S. Mjalli and M. Saleem, *J. Electrochem. Soc.*, 2011, **158**, R55-R79.
89. D. N. Buckley, X. Gao, R. P. Lynch, N. Quill and M. J. Leahy, *J. Electrochem. Soc.*, 2014, **161**, A524-A534.
90. S. M. Haile, *Acta Mater.*, 2003, **51**, 5981-6000.
91. J. R. Varcoe, P. Atanassov, D. R. Dekel, A. M. Herring, M. A. Hickner, P. A. Kohl, A. R. Kucernak, W. E. Mustain, K. Nijmeijer, K. Scott, T. Xu and L. Zhuang, *Energy Environ. Sci.*, 2014, **7**, 3135-3191.
92. Y. Bouhadana, M. Ben-Tzion, A. Soffer and D. Aurbach, *Desalination*, 2011, **268**, 253-261.
93. L. Han, K. G. Karthikeyan, M. A. Anderson, J. J. Wouters and K. B. Gregory, *Electrochim. Acta*, 2013, **90**, 573-581.
94. J. Kang, T. Kim, K. Jo and J. Yoon, *Desalination*, 2014, **352**, 52-57.